Structure of melt-quenched $AgIn_3Te_5$

C. Rangasami
Department of Physics, Indian Institute of Technology Madras, Chennai 600036, India

P. Malar and T. Osipowicz
Centre for Ion Beam Applications, Department of Physics, National University of Singapore, Singapore 17542, Singapore

Mahaveer K. Jain and S. Kasiviswanathan[a)]
Department of Physics, Indian Institute of Technology Madras, Chennai 600036, India

(Received 10 September 2010; accepted 5 March 2011)

Polycrystalline $AgIn_3Te_5$ synthesized by melt-quench technique has been analyzed using proton induced X-ray emission (PIXE), X-ray diffraction (XRD), and selected area electron diffraction. PIXE analysis yielded the content of Ag, In, and Te, respectively, to be 9.76%, 31.18%, and 59.05% by weight. Structure refinement was carried out considering those space groups from I- and P-type tetragonal systems which possess $\bar{4}$ symmetry and preserve the anion sublattice arrangement of the chalcopyrite structure (space group: $I\bar{4}2d$) as well. The results showed that $AgIn_3Te_5$ synthesized by melt-quench method crystallizes with P-type tetragonal structure (space group: $P\bar{4}2c$; unit-cell parameters $a = 6.2443(8)$ and $c = 12.5058(4)$ Å), the presence of which was corroborated by selected area electron diffraction studies. © *2011 International Centre for Diffraction Data.*
[DOI: 10.1154/1.3624887]

Key words: $AgIn_3Te_5$, Rietveld refinement, P-type tetragonal, electron diffraction, PIXE

I. INTRODUCTION

Ag-III-VI_2 based ternary and quaternary chalcopyrite semiconductors have been widely investigated because of their potential application in photovoltaics and nonlinear optics. For example, $AgGaTe_2$ (band gap 1.16 eV) thin-film based solar cells with efficiency of 4.8% at laboratory scale have been demonstrated (Mandal *et al*., 2003). Efficiency of 7.3% has been reported (Yamada *et al*., 2006) for a tandem solar cell with an $AgInGaSe_2$ absorber layer. $AgGaSe_2$, another compound of this family, exhibits a large nonlinear optical coefficient and high transmission in the IR region (Xue *et al*., 2000). In fact, $AgGaSe_2$ crystals for second harmonic generation in the IR region are commercially available (EKSPLA, 2011). When the occupancy of cations in the ideal chalcopyrite lattice is disturbed, a series of compounds with general formula $A^{I}B^{III}_{2n+1}C^{VI}_{3n+2}$, where $n = 0$, 1, 2, have been reported to stabilize (Zhang *et al*., 1997). These compounds have been studied with equal interest, ever since the experimental observation of $CuIn_3Se_5$ as a segregated phase over $CuInSe_2$ film surface (Schmid *et al*., 1993). While a number of Cu based compounds have been investigated, Ag based systems have attracted much less attention. Reported work on Ag-based vacancy compounds, mainly concern with Ag-III_5-VI_8. The exception being $AgIn_3Te_5$, on which preliminary work was done by O'Kane and Mason (1964), and in fact, its structure has not been resolved yet. Since, the structure of $AgInTe_2$ ($I\bar{4}2d$) and $AgIn_5Te_8$ ($P\bar{4}2m$) have been understood fairly well (Diaz *et al*., 2000; Sanchez *et al*., 2005), it is of interest to investigate $AgIn_3Te_5$, which is located in between the above two on the Ag_2Te-In_2Te_3 tie line in the Ag-In-Te ternary phase diagram (Chiang *et al*., 1967). The present investigation aims at determining the structure of melt-quenched $AgIn_3Te_5$ unambiguously through proton induced X-ray emission (PIXE), X-ray diffraction (XRD) and selected area electron diffraction studies.

The isostructural nature of Cu and Ag based compounds in the I-III-VI_2 family implies that the structure of $AgIn_3Te_5$ may be related to that of $CuIn_3VI_5$. Therefore, it is not unreasonable to consider the structures suggested for $CuIn_3VI_5$ compounds based on Rietveld and electron diffraction analysis. Thiogallate, stannite, and P-type tetragonal structures have been proposed for Cu-In-Se, a widely studied system with compositional ratio close to 1:3:5. Tseng and Wert (1989) have suggested thiogallate structure (space group: $I\bar{4}$) based on electron diffraction data of commercially grown sample with composition $CuIn_3Se_{5.33}$. A similar conclusion has been arrived at by Bodnar *et al*. (2006) from an XRD study of single crystal $CuIn_3Se_5$. Hanada *et al*. (1997) have concluded that $CuIn_3Se_5$ crystallizes with stannite structure (space group: $I\bar{4}2m$) based on XRD and electron diffraction analysis of $CuIn_3Se_5$ powder obtained from ingots grown by air cooling the melt. Rietveld refinement of crystal structure (Paszkowicz *et al*., 2004) using XRD data of $CuIn_3Se_5$ powder, obtained from single crystal $CuIn_3Se_5$, has led to similar conclusions as well. P-type tetragonal structure with $P\bar{4}2c$ space group has also been suggested by several authors. The studies include Rietveld refinement of crystal structures using: (i) XRD data of $CuIn_3Se_5$ single crystal quenched from 1023 K into water (Honle *et al*., 1988) and (ii) XRD data of $CuIn_2Se_{3.5}$ and $CuIn_3Se_5$ powders obtained from furnace cooled ingots

a)Author to whom correspondence should be addressed. Electronic mail: kasi@iitm.ac.in

(Merino *et al*., 2000) as well as electron diffraction study of single crystal $CuIn_3Se_5$ grown from vertical gradient freeze method (Tham *et al*., 2000). On the other hand, for the relatively less studied $CuIn_3Te_5$, XRD analysis (Marin *et al*., 2000) of $CuIn_3Te_5$ powder obtained from ingots grown by vertical Bridgman method has yielded a tetragonal chalcopyrite related structure, while Rietveld refinement of crystal structure using XRD data of $CuIn_3Te_5$ powder taken from ingots quenched from 1358 to 473 K has yielded P-type tetragonal structure with $P\bar{4}2c$ space group (Diaz *et al*., 2005).

It may be understood from the above observations that the structure of $CuIn_3Se_5$ and $CuIn_3Te_5$ depends on changes in composition as well as on the thermal cycle followed for sample synthesis. It may also be inferred that the structure analysis of I-In_3-VI_5 compounds, in general, is not straight forward and an exhaustive study is required before any conclusion can be drawn. Accordingly, while refining the structure of $AgIn_3Te_5$, we have considered all space groups in I- and P-type tetragonal systems, which possess $\bar{4}$ symmetry and also preserve the anion sublattice arrangement of the chalcopyrite structure. We have also corroborated the Rietveld refinement results using selected area electron diffraction measurements.

II. EXPERIMENTAL

A. Synthesis of bulk $AgIn_3Te_5$

Polycrystalline $AgIn_3Te_5$ was synthesized by melt-quench technique, which involved fusion of constituent elements and subsequent quenching in water. 5N purity Ag, In, and Te pieces with compositional ratio 1:3:5 and total mass of about ~5 g were taken in a cleaned quartz ampoule, which was then evacuated to a pressure of $\sim 5 \times 10^{-6}$ mbar and sealed. The sealed ampoule was heated in a vertical tubular furnace, the temperature of which was controlled to an accuracy of ±2 K. The furnace temperature was initially increased to 523 K at a rate of 4 K per min and was maintained at this temperature for 3 h in order to allow the exothermic reaction between In and Te to take place at a controlled rate. Heating was continued at the same rate up to 1273 K, which is higher than the melting points of the constituent elements. The charge in the ampoule was allowed to react in this molten state for 60 h with intermittent shaking in order to improve the homogeneity. Finally, the ampoule with the charge in the molten state was quenched in water. The ingot thus obtained was polycrystalline and was black in color with shiny surface.

B. Characterization of $AgIn_3Te_5$

1. PIXE measurement

PIXE measurements were performed using tandem pelletron accelerator facility available at the Centre for Ion Beam Analysis, National University of Singapore, Singapore. The sample for PIXE measurements was in the form of pellet (thickness ~1 mm and diameter 8 mm) made out of $AgIn_3Te_5$ powder. The sample was irradiated with collimated proton beam of energy 2 MeV, and the spectra were recorded with a maximum beam current of ~6 nA. The characteristic X-rays emitted from the sample were detected by a liquid N_2 cooled Si(Li) detector having a resolution of 170 eV at 5.9 keV. The detector was kept at an angle of 170° with respect to the incident beam and the characteristic X-rays were collected through a 50-μm thick Mylar window. The spectra were recorded using a Canberra series S-100 multichannel analyzer and were analyzed using the software "GUPIX" (Campbell *et al*., 2000) in order to determine the elemental concentrations. A digital filter in the software was used to remove the background in the experimental spectra. GUPIX uses a nonlinear least square procedure to fit the experimental data and converts the intensities of peaks into concentration of the respective constituent elements. The main experimental parameters, which are needed for the analysis, are incident ion energy, experimental geometry, detector details, filter details, the instrumental constant H, and the collected charge.

2. XRD measurement

Powder X-ray diffraction measurements were made at 298 K using a PANalytical (model-X'Pert PRO, equipped with X'Celerator detector) XRD unit with Cu- $K\alpha$ radiation source in the 2θ range 10 to 130° with step size of 0.0170° 2θ and integration time of ~40 s. The X-ray generator was operated at 40 kV and 30 mA, and the wavelengths of $K\alpha_1$ and $K\alpha_2$ lines were 1.54060 and 1.54443 Å, respectively. Theta compensating slit was fixed at 1°, and K_β lines present in the diffracted beam were filtered using a nickel filter. Prior to the measurements, the XRD unit was calibrated with silicon (external) standard. Specimen (mortar and pestle ground powder) for XRD measurements was taken in an aluminum well and was gently pressed (without affecting its random orientation) to present a smooth flat surface. Rietveld refinement was carried out using the software GSAS (Larson and von Dreele, 2004) supported by EXPGUI graphical user interface, which allows simultaneous refinement of two wavelengths ($K\alpha_1$and $K\alpha_2$ with intensity ratio 0.5, in the present case). Shifted Chebyschev polynomial was used to describe the background and a Pseudo-Voigt profile function was used to model the peak shapes. The quality of fit was described by the discrepancy factors (Young, 1993) R_p, R_{wp}, R_{exp}, R_F, and χ^2, the goodness of fit (GOF).

3. Electron diffraction measurement

Selected area electron diffraction measurements were made at different zone axis using a Philips CM-12 transmission electron microscope with an accelerating potential of 120 kV and a beam current of a few μA. The diameter of the probing electron beam was about 150 nm. For TEM measurements, fine particles of $AgIn_3Te_5$ were collected on carbon coated copper grids from a solution consisting of $AgIn_3Te_5$ powder dispersed in acetone/methanol.

III. RESULTS AND DISCUSSION

A. PIXE analysis

A typical 2 MeV PIXE spectrum of bulk $AgIn_3Te_5$ is shown in Figure 1. The inset to Figure 1 shows, on an

https://doi.org/10.1154/1.3624887 Published online by Cambridge University Press

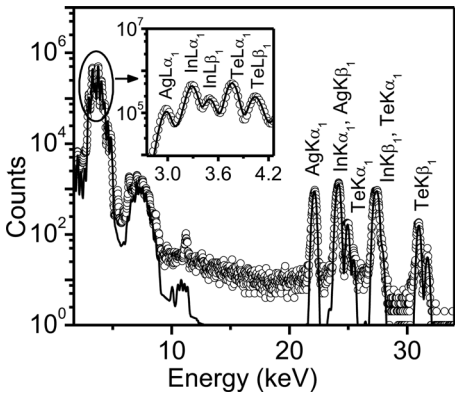

Figure 1. Typical PIXE spectrum of bulk $AgIn_3Te_5$. The circles represent experimental data and the continuous line denotes the calculated curve. The inset shows the spectrum in the range 2.7 to 4.25 keV, on an expanded scale.

expanded scale, the region between 2.7 and 4.3 eV. The characteristic X-ray lines from the constituent elements are marked in the spectrum for convenience. The instrument constant and energy calibration parameters were obtained using a standard sample (quartz), which emitted both *K* and *L* X-ray lines in the energy range 2 to 30 keV. Assuming bulk $AgIn_3Te_5$ as a matrix consisting of Ag, In, and Te with unknown ratio, a thick target PIXE analysis was carried out. The weights (in percentage) of Ag, In, and Te determined from the analysis are 9.76, 31.18, and 59.05, respectively, which show that the synthesized material is near stoichiometric.

B. Rietveld refinement

1. Structure refinement based on $I\bar{4}$, $I\bar{4}2m$, and $P\bar{4}2c$ space groups

Powder diffraction data (symbols) of $AgIn_3Te_5$ is shown in Figure 2. Rietveld refinement was initiated assuming thiogallate structure with $I\bar{4}$ space group. In this structure, the atomic position 2a at (0, 0, 0) is shared by both Ag and In atoms, whereas the positions 2b at (0, 0, 1/2), 2c at (0, 1/2, 1/4) and 2d at (0, 1/2, 3/4) are occupied by In atoms. Te atoms occupy the site 8g at (*x*, *y*, *z*), where *x*, *y*, and *z*

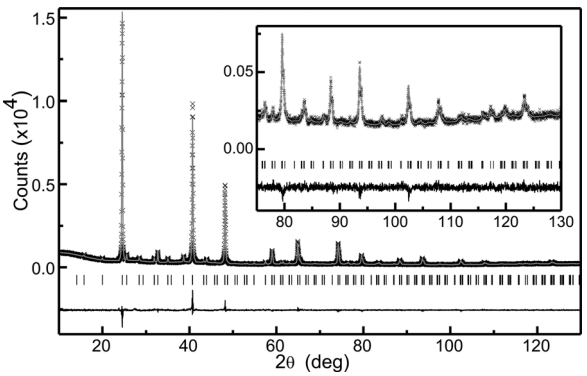

Figure 2. Experimental XRD pattern and the results of Rietveld refinement for $AgIn_3Te_5$. The inset shows the data in the range 85° to 130°, on an expanded scale. The crosses and the overlying solid line represent the experimental data and the calculated profile respectively. The short vertical markers indicate possible Bragg reflections whereas the bottom curve denotes the difference between the experimental and calculated data.

are free parameters. The assigned occupancies were (0.8Ag + 0.2In) at 2a, 1 at 2b, 1 at 2c, 0.2 at 2d, and 1 at 8g. It is to be noted here that all Rietveld refinements have been carried out assuming the ideal compositional ratio (1:3:5) as the composition of $AgIn_3Te_5$ is found to be near stoichiometric. The refinement converged satisfactorily to $R_{wp} = 7.53\%$ (*GOF*: 2.031). The calculated pattern, however, exhibited an additional reflection 002, the structure factor of which is $1.6f_{Ag}$, where f_{Ag} is Ag atomic scattering factor. Since the 002 reflection was not observed in the experimental pattern, refinement was performed with redistributed In occupancy (0.1 at 2a and 0.3 at 2d) that reduces the 002 reflection structure factor to $1.6f_{Ag} - 0.4f_{In}$, where, f_{In} is the atomic scattering factor for In. The refinement converged with a marginal reduction in R_{wp} value (7.38%, *GOF*: 1.954), but the anion positional parameters had to be kept fixed during the refinement.

Refinement was continued, assuming stannite structure with $I\bar{4}2m$ space group. In the unit cell, Ag atoms occupy 2a at (0, 0, 0), In atoms occupy 2b at (0, 0, 1/2) and 4d at (0, 1/2, 1/4), while Te atoms occupy 8i at (*x*, *y*, *z*). The assigned site occupancies were 0.8 at 2a, 0.4 at 2b, 1 at 4d, and 1 at 8i. The refinement converged to $R_{wp} = 6.38\%$ (*GOF*: 1.463), which is lower than that obtained for the refinement done assuming $I\bar{4}$ space group. However, the calculated pattern showed a low-intensity additional reflection 002, similar to the previous refinement. In order to verify if reduction in the intensity of 002 reflection would improve R_{wp}, refinement was performed by reducing the structure factor from $1.6f_{Ag} - 3.2f_{In}$ to $1.6fAg - 2.6f_{In}$ by redistributing In occupancy (0.55 at 2b, 0.925 at 4d) and leaving Ag and Te occupancies and composition unaltered. However, the refinement converged to higher value of R_{wp} (6.62%, *GOF*: 1.575), suggesting that the quality of refinement decreases.

Refinement was continued further assuming P-type tetragonal structure with $P\bar{4}2c$ space group. In the unit cell, Ag atoms occupy 2e at (0, 0, 0), In atoms occupy 2b at (1/2, 0, 1/4), 2d at (0, 1/2, 1/4) and 2f at (1/2, 1/2, 0), and Te atoms occupy 8n at (*x*, *y*, *z*). Vacancies are assumed to be present at the Ag site (2e) and the In site (2b). The refinement converged satisfactorily with $R_{wp} = 6.09\%$ (*GOF*: 1.328), which is the lowest among the R_{wp} values obtained so far. The optimized occupancies are 0.8 at 2e, 0.4 at 2b, 1 at 2f, 1 at 2d, and 1 at 8n. The results are presented in Figure 2 along with the experimental pattern. Unlike in the previous two cases, the calculated pattern did not contain any additional peaks. Further, all peaks observed in the experimental XRD pattern were found to obey the general reflection conditions for the space group $P\bar{4}2c$ given in the International Tables of X-ray Crystallography (Henry and Lonsdale, 1965). The unit-cell parameters obtained are $a = 6.2443(8)$ and $c = 12.5058(4)$ Å, with a tetragonal distortion $(\eta = c/2a) \sim 1.001$. The refined structural parameters are given in Table I.

The experimental and calculated powder diffraction data for bulk $AgIn_3Te_5$ synthesized by melt-quench method is listed in Table II. For the sake of brevity, only the reflections with relative intensity more than 0.3% are considered while forming Table II. The reflection with the highest intensity, 112, is observed at $2\theta = 24.556°$ and is mainly due

https://doi.org/10.1154/1.3624887 Published online by Cambridge University Press

TABLE I. Refined structure parameters for $AgIn_3Te_5$ synthesized by melt-quench method. Structure: P-type tetragonal, space group: $P\bar{4}2c$, unit-cell parameters: $a = 6.2443(8)$ and $c = 12.5058(4)$ Å, unit-cell formula weight = 1744.525, and density = 5.491 gm/cm^3. The discrepancy factors are $R_p = 4.75\%$, $R_{wp} = 6.09\%$, $R_{exp} = 5.28\%$, and $R_F{}^2 = 7.22\%$. The goodness of fit, $\chi^2 = 1.328$.

Atom	Wyckoff position	Atomic position (x,y,z)	Occupancy	Isotropic thermal parameter (Uiso) Å^2
Ag	2e	0, 0, 0	0.8	0.02048
In1	2b	1/2, 0, 1/4	0.4	0.05239
In2	2f	1/2, 1/2, 0	1	0.02762
In3	2d	0, 1/2, 1/4	1	0.02895
Te	8n	0.261, 0.225, 0.133	1	0.03059
	Bond length (Å)			Bond angle (°)
Ag-Te		2.72434(4)	Te-Ag- Te	112.035(1)
				104.456(2)
In1-Te		2.51435(3)	In1-Te-In2	111.715(1)
In2-Te		2.82017(4)	In1-Te-In3	112.889(2)
In3-Te		2.78105(3)	In2-Te-In3	104.151(1)
			Te-In1-Te	112.031(1)
				109.132(1)
				107.287(1)
			Te-In2-Te	110.494(1)
				107.444(2)
			Te-In3-Te	116.776(2)
				108.155(1)
				103.763(1)
			Ag-Te-In1	114.948(1)
			Ag-Te-In2	105.553(2)
			Ag-Te-In3	106.747(1)

to anion sublattice as in $AgInTe_2$. Reflections such as 202, 114, 212, 214, 306, 334, and 426 are not allowed as per the general reflection conditions for chalcopyrite structure. They are unique to off-stoichiometric or defect chalcopyrite structure. Reflections with extinction condition $h+k+l=2n+1$ are characteristic of P-type tetragonal class while those with extinction condition $h+k+l=2n$ are allowed for both P- and I-type tetragonal systems. Specifically, reflections which obey the conditions, $l=4n$ (with odd h, k-indices) or $l=4n+2$ (with even, h, k-indices) are expected for defect I-type structure. For P-type defect structure, reflections with condition $l=4n+2$ (with odd/even h, k-indices) are expected in addition. Thus, for instance 212, the highest intensity reflection among these additional ones is expected for $P\bar{4}2c$ alone. The above observations clearly favor $P\bar{4}2c$ space group over $I\bar{4}$ and $I\bar{4}2m$ space groups. However, choice of $P\bar{4}2c$ space group without further consideration is not possible at this stage since the experimental powder XRD data did not contain all reflections expected for $P\bar{4}2c$ space group. The 002 reflection for instance, although allowed in $P\bar{4}2c$ space group, was absent in the experimental XRD pattern. The reason for this may be that either these characteristic reflections are too weak to contribute or the structure itself is different. In order to eliminate the latter possibility, it is essential to consider the space groups in P- and I-type tetragonal systems with $\bar{4}$ symmetry, in general.

2. Discussion on other space groups in P- and I-type tetragonal systems with $\bar{4}$ symmetry

The remaining space groups with $\bar{4}$ symmetry in the P-type tetragonal system are $P\bar{4}$, $P\bar{4}2m$, $P\bar{4}2_1c$, $P\bar{4}2_1m$, $P\bar{4}m2$, $P\bar{4}c2$, $P\bar{4}n2$, and $P\bar{4}b2$ and those in the I-type tetragonal system are $I\bar{4}m2$ and $I\bar{4}c2$ (Henry and Lonsdale, 1965). However, not all of them need to be considered for the structure refinement of the title compound. This is because, although several structures have been proposed for I-III_3-VI_5 defect compounds, common to all of them is that they are tetragonal with the anion sublattice remaining same as that in a chalcopyrite unit cell. This requirement restricts the available space groups to $P\bar{4}$, $P\bar{4}2m$, $P\bar{4}2_1m$, and $P\bar{4}2_1c$. The rest of them ($P\bar{4}m2$, $P\bar{4}c2$, $P\bar{4}n2$, and $P\bar{4}b2$ space groups in P-type tetragonal system and $I\bar{4}m2$ and $I\bar{4}c2$ space groups in I-type tetragonal system) can be safely excluded from the analysis as they do not preserve the anion sublattice.

Structure refinement performed assuming $P\bar{4}$ space group with Ag on 1a at (0, 0, 0) and on 1b at (0, 0, 1/2), In on 1c at (1/2, 1/2, 0), 1d at (1/2, 1/2, 1/2), 2g at (0, 1/2, 1/4) and 2g at (0, 1/2, 3/4), and Te on 4h at (x, y, z) and 4h at (x, y, z+1/2) was found to converge only with fixed anion positional parameters. The minimum R_{wp} obtained was 7.92% (*GOF*: 2.249, site occupancy factors: 0.9 at 1a, 0.7 at 1b, 0.4 at 1c and 1d, 1 at 2g and 1 at 4h). In $P\bar{4}2m$ space group, Ag occupies 1a and 1c, respectively, at (0, 0, 0) and (0, 0, 1/2), In occupies 1b at (1/2, 1/2, 1/2), 1d at (1/2, 1/2, 0), and 4m at (0, 1/2, 1/4), and Te occupies 4n at (x, x, z) and 4n at (x, x, z+1/2). The minimum possible R_{wp} obtained from structure refinement was 8.21% (GOF: 2.420, site occupancy factors: 0.6 at 1a, 1 at 1c, 0.23 at 1b, 0.85 at 1d, 0.93 at 4m, and 1at 4n). In $P\bar{4}2_1m$ space group, the atomic positions in the unit cell are Ag on 2a at (0, 0, 0), In on 2b at (0, 0, 1/2), 2c at (0, 1/2, 1/4), and 2c at (0, 1/2, 3/4), and Te on 4e at (x, 1/2+x, z) and 4e at (x, 1/2+x, z+1/2). The refinement converged to

https://doi.org/10.1154/1.3624887 Published online by Cambridge University Press

TABLE II. Powder XRD data for $AgIn_3Te_5$ synthesized by melt-quench method. The space group is $P\bar{4}2c$. Reflections with relative peak heights <0.3% in the experimental data are not included in the table. Values of $2\theta_{obs}$, d_{obs} and I_{obs} are obtained from the experimental data using the software X'PERT HIGHSCORE PLUS, while values of $2\theta_{cal}$, d_{cal} and I_{cal} are calculated from refined unit-cell parameters and Miller indices (hkl).

$2\theta_{obs}$ (°)	d_{obs} (Å)	I_{obs} (%)	(*hkl*)	$2\theta_{cal}$ (°)	d_{cal} (Å)	I_{cal} (%)	$\Delta 2\theta$ (°)
15.735	5.6273	0.76	1 0 1	15.744	5.5866	0.64	−0.009
19.970	4.4426	0.97	1 1 0	19.987	4.4154	0.43	−0.017
24.541	3.6245	100.00	1 1 2	24.556	3.6068	100.00	−0.015
25.549	3.4837	2.43	1 0 3	25.567	3.4670	2.95	−0.018
28.360	3.1445	1.15	0 0 4	28.419	3.1265	0.62	−0.059
28.464	3.1333	1.67	2 0 0	28.459	3.1222	0.94	0.005
31.898	2.8033	1.98	2 0 2	31.907	2.7933	1.67	−0.009
32.709	2.7357	4.47	2 1 1	32.727	2.7254	5.09	−0.018
34.967	2.5640	1.34	1 1 4	35.034	2.5516	1.42	−0.067
35.074	2.5564	2.06	2 1 2	35.059	2.5498	0.48	0.015
38.628	2.3290	2.97	1 0 5	38.643	2.3218	1.14	−0.015
38.669	2.3266	2.67	2 1 3	38.674	2.3201	1.70	−0.005
40.623	2.2191	43.89	2 0 4	40.704	2.2092	51.27	−0.081
40.717	2.2142	72.24	2 2 0	40.733	2.2077	25.01	−0.016
43.972	2.0576	2.16	3 0 1	43.961	2.0532	1.62	0.011
48.033	1.8926	12.46	1 1 6	48.135	1.8849	14.75	−0.102
48.164	1.8878	39.39	3 1 2	48.186	1.8830	28.20	−0.023
48.774	1.8656	1.08	2 1 5	48.734	1.8631	0.49	0.040
54.916	1.6706	0.30	3 1 4	54.844	1.6695	0.47	0.072
57.465	1.6024	1.26	3 2 3	57.475	1.5993	1.90	−0.011
58.963	1.5652	6.36	0 0 8	58.935	1.5632	3.24	0.027
59.011	1.5641	7.00	4 0 0	59.024	1.5611	6.07	−0.013
61.008	1.5175	0.70	2 2 6	60.985	1.5156	0.57	0.023
61.506	1.5064	1.23	2 1 7	61.464	1.5049	0.53	0.042
61.544	1.5056	0.96	4 1 1	61.530	1.5035	0.62	0.014
62.949	1.4753	0.67	1 1 8	62.921	1.4736	0.67	0.028
64.903	1.4356	11.30	3 1 6	64.898	1.4335	9.49	0.005
64.987	1.4339	5.34	3 3 2	64.941	1.4326	4.69	0.046
65.403	1.4258	2.54	3 2 5	65.393	1.4238	1.45	0.010
65.416	1.4255	2.49	4 1 3	65.414	1.4234	1.21	0.002
72.816	1.2978	0.37	4 1 5	72.857	1.2955	0.84	−0.041
74.147	1.2778	8.58	2 2 8	74.172	1.2758	5.11	−0.025
74.212	1.2768	11.39	4 2 4	74.231	1.2749	10.05	−0.019
76.441	1.2450	1.00	4 3 1	76.502	1.2427	0.87	−0.061
77.799	1.2267	0.43	3 1 8	77.765	1.2257	0.68	0.034
79.560	1.2039	4.04	1 1 10	79.499	1.2033	2.00	0.061
79.570	1.2038	3.97	3 3 6	79.577	1.2023	1.82	−0.007
79.594	1.2035	3.55	5 1 2	79.616	1.2018	3.63	−0.022
83.119	1.1612	0.51	2 0 10	83.027	1.1609	0.55	0.092
83.429	1.1576	0.64	4 1 7	83.527	1.1552	0.48	−0.099
83.581	1.1559	1.18	5 2 1	83.585	1.1546	0.90	−0.004
88.341	1.1055	2.43	4 0 8	88.317	1.1046	2.72	0.024
88.366	1.1052	2.31	4 4 0	88.394	1.1039	1.32	−0.028
88.468	1.1042	1.76	3 1 10	88.507	1.0565	2.05	−0.039
93.560	1.0570	2.59	5 1 6	93.584	1.0559	1.99	−0.024
93.598	1.0567	2.66	5 3 2	93.622	1.0555	1.95	−0.024
101.136	0.9973	0.45	6 1 3	101.095	0.9968	0.60	0.041
102.246	0.9895	1.11	2 0 12	102.266	0.9885	1.69	−0.020
102.365	0.9886	1.94	6 0 4	102.423	0.9875	1.44	−0.058
102.520	0.9876	1.01	6 2 0	102.443	0.9873	1.38	0.077
107.801	0.9534	1.41	3 3 10	107.741	0.9530	0.89	0.060
107.843	0.9531	1.14	5 3 6	107.821	0.9525	1.71	0.022
115.824	0.9092	0.45	5 4 5	115.830	0.9086	0.44	−0.006
117.226	0.9023	0.63	4 4 8	117.241	0.9017	1.30	−0.015
119.679	0.8909	0.45	5 2 9	119.700	0.8903	0.51	−0.021
119.856	0.8901	0.71	6 1 7	119.744	0.8901	0.41	0.112
123.114	0.8761	1.00	1 1 14	123.118	0.8755	0.59	−0.004
123.290	0.8753	1.29	5 1 10	123.256	0.8750	1.21	0.034
123.420	0.8748	0.97	7 1 2	123.394	0.8744	1.07	0.026

R_{wp}= 7.65% (*GOF*: 2.098, site occupancy factors: 0.8 at 2a, 1 at 2b, 0.4 for $z = 1/4$ and 1 for $z = 3/4$ at 2c, and 1 at 4e).

In all the above refinements, the calculated patterns exhibited low-intensity *hhl* reflections 002, 003/111, and 113, regardless of Ag and In site occupancies. In addition, the refinements based on these space groups yielded higher R_{wp} values compared to that obtained for $P\bar{4}2c$ space group. Finally, structure refinement assuming $P\bar{4}2_1c$ space group was carried out with Ag on 2a at (0, 0, 0), In on 2b at (0, 0, 1/2) and 4d at (0, 1/2, 1/4), and Te on 8e at (*x*, *y*, *z*). The refinement converged only with fixed anion positional parameters, and the minimum R_{wp} obtained was 8.94% (*GOF*: 2.868, site occupancy factors: 0.8 at 2a, 0.5 at 2b, 0.95 at 4d, and 1 at 8e), which is higher than that obtained for $P\bar{4}2c$. Further, the calculated pattern was always found to contain a 002 peak with finite intensity, regardless of the occupancies at In sites.

3. Discussion on hhl reflections

In all refinements except that based on $P\bar{4}2c$ space group, the 002 reflection with observable intensity was present in the calculated pattern. In addition, the refinements with $P\bar{4}$, $P\bar{4}2m$ and $P\bar{4}2_1m$ space groups, the 003/111 and 113 reflections appeared in the calculated pattern. The 002 reflection is characteristic of defect phases (extinction condition $l = 4n + 2$ with even *h, k* indices) and is allowed in the space groups $P\bar{4}2c$ and $I\bar{4}2m$ under the general reflection condition *hhl*: $l = 2n$, while in $I\bar{4}$ space group, it is allowed under the condition $h+k+l = 2n$. The reflections 003/111 and 113 are allowed in addition to 002 in $P\bar{4}$, $P\bar{4}2m$, and $P\bar{4}2_1m$ space groups under the condition *hhl*: l = odd or even. In order to verify if the intensities of these reflections are really negligible in the experimental data, high-resolution scans (step size: 0.002° and acquisition time 60 s) were taken. Figures 3(a) and 3(b) are examples of high-resolution scans taken around 14° and 21°, respectively. The large circles in Figures 3(a) and 3(b) indicate the regions where the 002 and 003/111 reflections are expected. Absence of any feature indicates that these reflections, if present, have negligibly small relative intensities. The reason for the absence of the 002 reflection may be that its structure factor in $P\bar{4}2c$ space group ($1.6f_{Ag} - 0.8f_{In}$) has the least value among the structure factors in the space groups considered and therefore its intensity can be annulled easily, while maintaining stoichiometry. The absence of 003/111 reflections in addition to 002 indicates that the space group $P\bar{4}$ or $P\bar{4}2m$ or $P\bar{4}2_1m$ is not suitable. Figure 3(c) shows powder diffraction data around the region in which the 114 peak appears. Deconvolution of the data clearly reveals the nearby 212 reflection, which is disallowed for the I-type tetragonal

https://doi.org/10.1154/1.3624887 Published online by Cambridge University Press

system. Although the 212 peak is close to the 114 peak, it could be resolved well in electron diffraction patterns, a discussion of which will appear in the latter sections. Thus, it may be concluded from the Rietveld analysis that among all space groups considered, $P\bar{4}2c$ is the most likely space group for near stoichiometric $AgIn_3Te_5$ synthesized by melt-quench technique.

4. Structure of $AgIn_3Te_5$

The choice of $P\bar{4}2c$ space group ensures that the anion sublattice remains undisturbed as that in chalcopyrite structure. The cationic sublattice is occupied by Ag and In atoms, and vacancies at four different Wyckoff positions (Table I) with no evidence of mixed occupancies of cations. The vacancies may be distributed statistically or arranged in a particular order. Further, the rearrangement of Ag and In atoms and the introduction of vacancies in cationic sublattice lead to the displacement of Te atoms (with 3 degrees of freedom) from their ideal position 1/4, 1/4, 1/8. Moreover, the refined Ag-Te bond length (2.72 Å) in $AgIn_3Te_5$ unit cell was found to be smaller compared to that (2.76 Å) in $AgInTe_2$ (Xue *et al.*, 2000), which may be attributed to the presence of Ag vacancies. Similar observations were made on $CuIn_3Te_5$ and $CuIn_3Se_5$ compounds by Rincon *et al.* (2000) and Paszkowicz *et al.*, (2004), respectively. Furthermore, the different bond lengths obtained between In and Te atoms can be explained on the basis of displacement and electronegativity of Te atoms, and the occupancies of In atoms.

Figure 4 shows the unit cell of $AgIn_3Te_5$, which was constructed with the refined structural parameters as guide. When the site occupancies are normalized to Te atom occupancy, the chemical formula of the compound can be written as $Ag_{0.8}In_{2.4}Te_4$ with two formula units in a single unit cell. The dotted lines represent the unit-cell boundary while the bonding between the atoms is shown by thick solid lines. It can be seen from Figure 4 that the unit cell has five different types of tetrahedral structures, viz., $(\square + Ag)$-Te_4, $(\square + In1)$-Te_4, In2-Te_4, In3-Te_4, and $(\square + AgIn_3)$-Te, where $\square$ denotes vacancy. The bond angles in the tetrahedra varied from 103.76° to 116.77°. However, the average bond angle in each of the tetrahedron was found to be close to the ideal value of 109.47°.

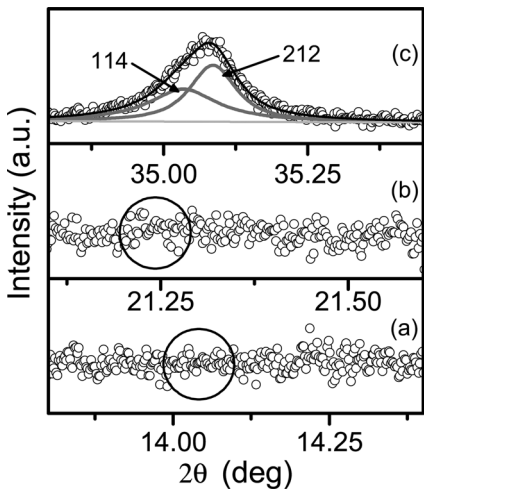

Figure 3. High resolution (step size: 0.002°, acquisition time 60 s) XRD data of $AgIn_3Te_5$ recorded in different 2θ ranges. The large circle in panel (a) marks the region where 002 reflection is expected, while that in panel (b) depicts the region where 003 reflection is expected. The presence of two closely spaced reflections (114 and 212) can be seen clearly in panel (c). In panel (c), the gray lines show the individual deconvolutions while the dark line shows the overall sum.

C. Electron diffraction analysis

Selected area electron diffraction patterns of $AgIn_3Te_5$ particles recorded along two different zone axes are shown in Figures 5(a) and 5(b). The zone axis for the pattern shown in Figure 5(a) is $[\bar{3}31]$ and that for the pattern shown in Figure 5(b) is $[22\bar{1}]$. A well-ordered array of spots observed in the patterns indicates the crystalline quality of the particle under investigation. The patterns were indexed following the usual procedure. The pattern indexed with the zone axis $[\bar{3}331]$ [Figure 5(a)] shows 103, $12\bar{3}$, 220 and 323 reflections while that indexed with the zone axis $[22\bar{1}]$ [Figure 5(b)] exhibits $\bar{2}20$, 204, 024, 102, and $\bar{1}22$ reflections. The spots corresponding to the reflections 102 and $\bar{1}22$ are weak in intensity [Figure 5(b)] when compared to the others and may be attributed to their small structure factors. The observed reflections may be categorized as follows. The reflections 220, $\bar{2}20$, 204, and 024 are typical of zinc blende lattice (extinction condition $h+k+l=2n$ and even l-indices). The reflections 103, $12\bar{3}$, and 323 are specifically from chalcopyrite lattice ($h+k+l=2n$ and odd l-indices). The reflections 102 and $\bar{1}22$ are unique to P-type tetragonal structure with $P\bar{4}2c$ space group. Thus, while the zone axis [$\bar{3}31$] limits

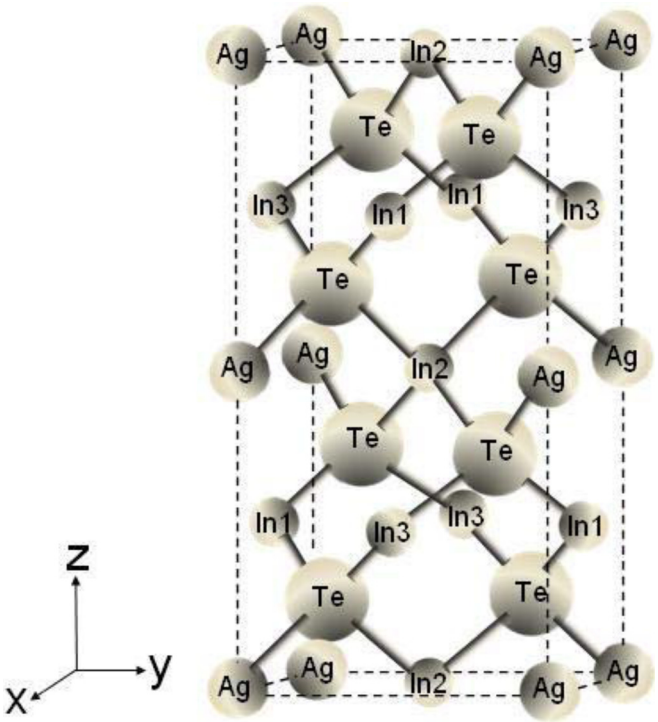

Figure 4. (Color online) Unit cell of $AgIn_3Te_5$ constructed using refined cell parameters as guide. Site occupancy factors of Ag, In1, In2, In3, and Te atoms are 0.8, 0.4, 1, 1, and 1, respectively. The dotted lines denote the cell boundary.

https://doi.org/10.1154/1.3624887 Published online by Cambridge University Press

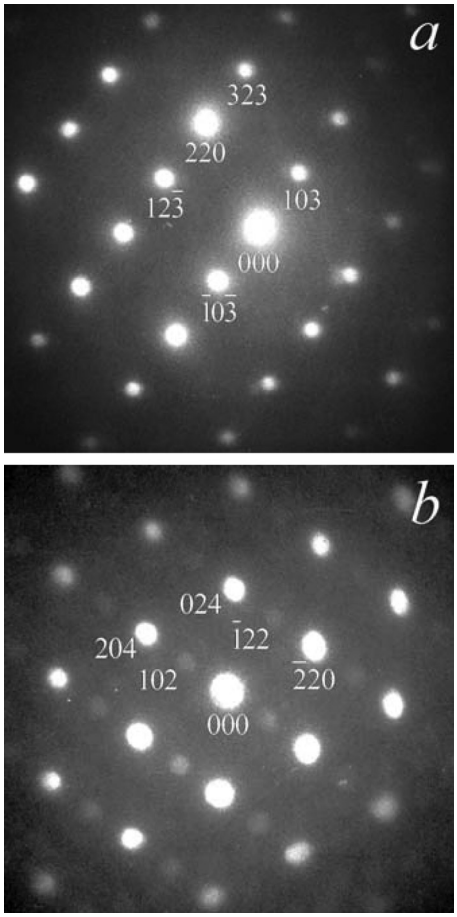

Figure 5. Electron diffraction patterns recorded on fine $AgIn_3Te_5$ particles. The zone axes are (a) [3̄31] and (b) [22$\bar{1}$].

the observable reflections [Figure 5(a)] to some of those from zinc blende and chalcopyrite lattices, the zone axis [22$\bar{1}$] allows some of the reflections, which are unique to P-type tetragonal structure to be observed as well. The presence of $\bar{1}22$ reflection (denoted 212 in the XRD pattern) corroborates well the conclusions drawn from Rietveld analysis on the existence of $P\bar{4}2c$. It is worth to note here that while the $\bar{1}22$ reflection could be identified uniquely through selected area electron diffraction pattern, it was close to the 114 reflection in the XRD pattern. The angular separation between 114 and 212 reflections in XRD pattern is determined by the tetragonal distortion. In the absence of tetragonal distortion they will be degenerate, but can still be resolved in electron diffraction pattern. Thus, from the combined analysis of PIXE, XRD, and electron diffraction, we can safely conclude that melt-quenched $AgIn_3Te_5$ with near stoichiometric composition crystallizes with $P\bar{4}2c$ space group.

IV. CONCLUSION

The structure of $AgIn_3Te_5$, which is synthesized by melt-quench method, has been analyzed using a combined study of PIXE, XRD, and electron diffraction. Composition analysis by PIXE has confirmed the near stoichiometric nature. Rietveld refinement of crystal structure has been done by considering the space groups $P\bar{4}$, $P\bar{4}2m$, $P\bar{4}2c$, $P\bar{4}2_1m$, $P\bar{4}2_1c$, $I\bar{4}$, and $I\bar{4}2m$, which preserve the anion sublattice arrangement of the chalcopyrite unit cell. The results have shown that near stoichiometric $AgIn_3Te_5$ synthesized by melt-quench method crystalizes with P-type tetragonal structure (space group: $P\bar{4}2c$), the existence of which has also been confirmed by selected area electron diffraction patterns.

ACKNOWLEDGMENTS

The authors wish to thank the reviewers for their constructive views, technical comments, and useful suggestions. One of the authors (C. Rangasami) gratefully acknowledges the All India Council for Technical Education (AICTE), Government of India for a Research Fellowship under the QIP scheme.

Bodnar, I. V., Vaipolin, A. A., Rud, V. Y., and Rud, Y. V. (**2006**). "Crystal structure of $CuIn_3Se_5$ and $CuIn_5Se_8$ ternary compounds," Tech. Phys. Lett. **32**, 1003–1005.

Campbell, J. L., Hopman, T. L., Maxwell, J. A., and Nejedly, Z. (**2000**). "The Guelph PIXE software package III: Alternative proton database," Nucl. Instrum. Methods B **170**, 193–204.

Chang, C. H., Wei, S. H., Johnson, J. W., Zhang, S. B., Leyarovska, N., Bunker, G., and Anderson, T. J. (**2003**). "Local structure of CuInSe2: X-ray absorption fine structure study and first-principles calculations," Phys. Rev. B **68**, 054108 (9).

Chiang, P. W., O'Kane, D. F., and Mason, D. R. (**1967**). "Phase diagram of the pseudo-binary system Ag_2Te-In_2Te_3 and semiconducting properties of $AgIn_9Te_{14}$," J. Electrochem. Soc. **114**, 759–760.

Diaz, M., De Chalbaud, L. M., Sagredo, V., Tinco, T., and Pineda, C. (**2000**). "Synchrotron structural study of $AgInTe_2$," Phys. Status Solidi B **220**, 281–284.

Diaz, R., Bisson, L., Agullo-Rueda, F., Abd Lefdil, M., and Rueda, F. (**2005**). "Effect of composition gradient on $CuIn_3Te_5$ single-crystal properties and micro-Raman and infrared spectroscopies," Appl. Phys. A **81** 433–438.

EKSPLA (**2011**) <http:/www.ekspla.com> [accessed 7/25/2011]

Hanada, T., Yamana, A., Nakamura, Y., Nittono, O., and Wada, T. (**1997**). "Crystal structure of $CuIn_3Se_5$ semiconductor studied using electron and X-ray diffractions," Jpn. J. Appl. Phys. **36**, L1494–L1497.

Honle, W., Kühn, G., and Boehnke, U. C. (**1988**). "Crystal structures of two quenched Cu-In-Se phases," Cryst. Res. Technol. **23**, 1347–1354.

International Tables for X-Ray Crystallography, Vol. I. Symmetry Groups, edited by N. F. M. Henry and K. Lonsdale (**1965**) (The Kynoch Press, Birmingham, England).

Larson, A. C. and Von Dreele, R. B. (**2004**). General Structure Analysis System (GSAS), Report LAUR 86-748, Los Alamos National Laboratory, Los Alamos, NM.

Mandal, K. C., Smirnov, A., Roy, U. N., and Burger, A. (**2003**). "Thermally evaporated $AgGaTe_2$ thin films for low-cost p-$AgGaTe_2$/n-Si heterojunction solar cells," Mater. Res. Soc. Symp. Proc. **744**, 131–136.

Marin, G., Delgado, J. M., Wasim, S. M., Rincon, C., Sanchez Perez, G., Mora, A. E., Bocaranda, P., and Henao, J. A. (**2000**). "Crystal growth and structural, electrical, and optical characterization of $CuIn_3Te_5$ and $CuGa_3Te_5$ ordered vacancy compounds," J. Appl. Phys. **87**, 7814–7819.

Merino, J. M., Mahanty, S., Leon, M., Diaz, R., Rueda, F., Martin de Vidales, J. L. (**2000**). "Structural characterization of $CuIn_2Se_{3.5}$, $CuIn_3Se_5$ and $CuIn_5Se_8$ compounds," Thin Solid Films **361–362**, 70–73.

O'Kane, D. F. and Mason, D. R. (**1964**). "Semiconducting properties of $AgIn_3Te_5$," J. Electrochem. Soc. 3, 546–549.

Paszkowicz, W., Lewandowska, R., and Bacewicz, R. (**2004**). "Rietveld refinement for $CuInSe_2$ and $CuIn_3Se_5$," J. Alloys Compd. **362**, 241–247.

Rincon, C., Wasim, S. M., Marin, G., Hernandez, E., Delgado, J. M., and Galibert, J. (**2000**). "Raman spectra of $CuInTe_2$, $CuIn_3Te_5$, and $CuIn_5Te_8$ ternary compounds," J. Appl. Phys. **88**, 3439–3444.

Sanchez, A., Melendez, L., Castro, J., Hernandez, J. A., Hernandez, E., and Durante Rincon, C. A. (**2005**). "Structural, optical, and electrical properties of $AgIn_5Te_8$," J. Appl. Phys. **97**, 053505(4).

Schmid, D., Ruckh, M., Granwald, F., and Schock, H. W. (**1993**). "Chalcopyrite/defect chalcopyrite hetrojunctions on the basis of $CuInSe_2$," J. Appl. Phys. **73**, 2902–2909.

https://doi.org/10.1154/1.3624887 Published online by Cambridge University Press

Tham, A. T., Su, D. S., Neumann, W., Schubert-Bischoff, P., Beliharz, C., and Benz, K. W. (**2000**). "Transmission electron microscopy study of $CuIn_3Se_5$," Cryst. Res. Technol. **35**, 823–830.

The Rietveld Method (IUCr Monograph on Crystallography, No. 5), Edited by R. A. Young (**1993**) (Oxford University Press, New York).

Tseng, B. H. and Wert, C. A. (**1989**). "Defect-ordered phases in a multi-phase Cu-In-Se material," J. Appl. Phys. **65**, 2254–2257.

Xue, D., Betzler, K., and Hesse, H. (**2000**). "Dielectric properties of I-III-VI_2-type chalcopyrite semiconductors," Phys. Rev. B **62**, 13546–13551.

Yamada, K., Hoshino, N., and Nakada, T. (**2006**). "Crystallographic and electrical properties of wide gap $Ag(In_{1-x}Ga_x)Se_2$ thin films and solar cells," Sci. Technol. Adv. Mater. **7**, 42–45.

Zhang, S. B., Wei, S. H., and Zunger, A. (**1997**). "Stabilizaion of ternary compounds via ordered arrays of defect pairs," Phys. Rev. Lett. **78**, 4059–4062.

https://doi.org/10.1154/1.3624887 Published online by Cambridge University Press